ARTICLE

Investigating the effect of species-specific calibration on the quantitative imaging of iron at mg kg^{-1} and selenium at µg kg^{-1} in tissue using laser ablation with ICP-QQQ-MS

Received 3rd February 2021,
Accepted 00th January 20xx

DOI: 10.1039/x0xx00000x

Kharmen Billimoria [a, b, c], David N. Douglas[a,d] Gonzalo Huelga-Suarez [a], Joanna F. Collingwood [c] and Heidi Goenaga-Infante [a]†

There is evidence that iron (Fe) and selenium (Se) are dysregulated in neurodegenerative diseases (ND). Disease-specific impacts on concentration distributions are anticipated for Fe (the most abundant transition metal), and Se (present at trace levels), necessitating imaging strategies that enable their simultaneous quantification in ND pre-clinical models or post-mortem samples. This paper describes methodology for the production of matrix-matched tissue homogenates containing both Fe and Se at pathophysiological levels and investigates their feasibility as calibration standards for quantitative imaging of these elements. For the first time the effect of elemental species-specific calibration on the quality of LA-ICP-MS data is evaluated by investigating whether tissue matched standards spiked with inorganic Fe and Se are suitable alternatives to those spiked with specific species (e.g. ferritin or selenoproteins). To achieve this, the correlation of the calibration graph slopes (inorganic versus metalloprotein-spiked) as well as the homogeneity of the calibration standards were monitored over a laser energy range of 1 to 6 $J \cdot cm^{-2}$. For Fe, such slopes were found to agree well within the associated measurement error. In contrast, the choice of calibrant for Se was observed to have a greater impact; at 1 $J \cdot cm^{-2}$ the regression slope for the selenoprotein calibration was approximately 36% less than that of inorganic Se calibration. Finally, the limit of detection of Se was improved 2-fold by mixing 25% (*v/v*) methanol with the laser-induced aerosol in a chamber prior to introduction into the ICP, making the simultaneous detection of both elements possible at physiologically relevant concentrations.

Keywords: species-specific calibration, LA-ICP-MS, iron and selenium in brain tissue, inorganic selenium and iron, selenoproteins, ferritin, matrix-matched calibrants

Introduction

Increase in life expectancy has led to a globally ageing population and as a consequence an increase in the prevalence of neurodegenerative diseases, including Alzheimer's disease (AD). Study of metal ions and metalloproteins in neurodegenerative disease pathology is an area of growing interest[1,2]. In this vein, methods capable of detecting changes in metal distribution in relation with disease progression in both clinical and post-mortem samples are in high demand. In these highly complex systems much remains to be understood about the association of particular metal elements with biomarkers of disease. Further understanding of the integral roles of metal ions in disease pathogenesis for disorders such as AD, may provide routes to develop more effective therapies[3].

Whilst the highly complex pathophysiology of AD is incompletely described, two widely recognised hallmarks of AD and related disorders, widely used in clinical research to further understanding in both diagnostic and therapeutic research, are an increased density of β-amyloid (Aβ) deposits (typically 'senile plaques') in the extracellular spaces in AD brain tissue compared with healthy tissue, and phosphorylated tau observed within neurons as neurofibrillary tangles (NFTs) [4,5].

Iron (Fe) dysregulation within the brain has been implicated in the excessive formation of reactive oxygen species (ROS) associated with Aβ plaque formation[6], protein aggregation and cell death[7]. There is scope for catalytic over-production of radical species when iron interacts with aggregating Aβ, but there is also the possibility that in the human brain Aβ binding of iron within plaques mitigates excess radical production[8], so it is important that these systems can be described accurately. In contrast, selenoproteins can act as antioxidants [9] and neuroprotectors by scavenging and/or binding to free radicals produced[10] thus potentially delaying the progression of AD[11]. For the purpose of comparison of Se and Fe distributions between healthy and diseased individuals as well as between different populations over time, methods that enable reliable quantification of changes in the elemental spatial distribution of specific brain regions as a response to disease status are urgently needed. In this vein, absolute rather than relative approaches are

[a] *LGC Ltd, Queens Road, Teddington, TW11 0LY, United Kingdom*
[b] *MAS-CDT, Department of Chemistry, University of Warwick, Coventry, CV4 7AL, United Kingdom*
[c] *School of Engineering, University of Warwick, Coventry, CV4 7AL, United Kingdom*
[d] *Current affiliation: Elemental Scientific Lasers LLC, 7 Avro Court Ermine Business Park, Huntingdon, Cambridge, PE29 6XS, United Kingdom*

† Corresponding author: Heidi.Goenaga-Infante@lgcgroup.com

also invaluable to distinguish whether a variation in the ICP-MS signal can be either correlated with a change of element concentration or considered a matrix effect.

To achieve this, one key remaining challenge is the large difference in concentrations at which these elements are present. Iron, the most abundant transition metal found in the brain, is distributed heterogeneously throughout different brain regions. It is also widely accepted that further Fe accumulation occurs with ageing[12]. A study by Ramos *et al* [13] on Fe distribution in healthy ageing brains reported the highest concentration of this element (between 800- 1500 mg kg^{-1} Fe) in regions such as putamen, globus pallidus and caudate nucleus located in the basal ganglia. The authors also reported an average Fe concentration of approximately 100 mg kg^{-1} in the medulla, one of the least abundant brain regions located in the cerebellum. In contrast Se, whilst essential to healthy brain function, is present at trace levels with a mean concentration of 0.9 mg kg^{-1} across 14 measured brain regions[14].

Laser ablation inductively coupled plasma mass spectrometry (LA-ICP-MS) imaging allows for quantification of element spatial distribution in the sample if appropriate protocols for sample preparation and mounting are undertaken[15]. Recent advancements in ablation cell design[16] and laser technology[17,18] have led to improvements in overall image trueness with developments focused on creating a balance between sensitivity, selectivity and faster analysis times[19].

Despite key advances in technology, absolute quantification by LA-ICPMS still suffers from matrix effects which potentially introduce bias affecting the accuracy of the imaging data[20]. This, combined with the lack of commercially available reference materials (RM) for method validation and/or a universal calibration procedure have resulted in several efforts by different groups to develop strategies for calibration and signal normalisation[21–23] which have been extensively reviewed over the last few decades[24–27].

One commonly used approach is the preparation of *in house* matrix-matched calibration standards, spiked with the analytes of interest. Since elemental fractionation is strongly dependent on the composition of the sample it is widely accepted that having the same, or as close as feasible, matrix for both samples and standards helps reduce bias introduced by fractionation or transportation effects[28]. Methodology for preparing matrix-matched tissue homogenates has been described in detail in many recent studies[29–31]. This approach focuses on ensuring that the overall matrix i.e. the type of tissue or substrate of the calibration standard closely matches that of the sample, but no special attention has been paid so far to the nature of the spike[32]. For the preparation of *in-house* matrix matched homogenates, the matrix has often been spiked with an inorganic salt solution, which does not closely match the species of the analyte in the biological tissue. However, metals such as Fe and Se in the brain are bound to complex moieties like proteins with specific metabolic functions.

This paper describes methodology for the production of matrix-matched pig brain homogenates containing both Fe and Se as well as studying their feasibility as calibration standards for quantitative imaging of these elements present at concentration levels which are different by several orders of magnitude. For the first time, the effect of species-specific calibration on the quality of LA-ICP-MS data is evaluated here by investigating whether tissue matched standards spiked with inorganic Fe and Se are feasible alternatives to those spiked with specific species (e.g. metalloproteins) for quantitative tissue imaging. This is achieved by looking at the correlation of the calibration graph slopes (inorganic versus metalloprotein-spiked) as well as the within-line relative standard deviation (RSD) over a range of laser fluences. Moreover, efforts to improve the limit of detection for Se were undertaken by adding carbon to the plasma through the mixing of methanol with the laser induced aerosol in a chamber prior to introduction into the ICP.

Experimental

Materials

Pig brain was sourced from an ethically reputable butcher (Brays & Sons, Tideford, Cornwall, UK), and as such categorised as a meat product. Inorganic spikes were prepared by dissolving $FeCl_2$ and $SeCl_4$ salts (99.99%, Sigma Aldrich, Dorset, UK) in ultrapure 18 MΩ water to yield spike stock solutions of *ca* 5000 and 10 mg·kg^{-1} respectively. Ferritin (equine spleen, F4503, Sigma Aldrich, Dorset, UK) was selected as the high molecular weight (19-21 kDa), Fe-related protein-species spike. The solution contained 6671 mg·kg^{-1} of Fe, as characterised *in house* using the double IDMS methodology reported elsewhere[33].

In the absence of a suitable well characterised standard of selenoprotein P (well known as brain-mediating protein), the choice of Se spike was a Se-containing protein mixture from the water soluble fraction of selenised yeast[33]. The choice was made with the purpose of having a stable source of protein-like selenium with the level of Se required for spiking the tissue at reduced cost. For preparation of the spike water-soluble proteins were extracted from 0.3 g of SELM-1 (NRC, Ottawa, CA) in 5 mL 0.01 % dithiothreitol. (DTT), sonicated for 4 hours with minimal light exposure, as detailed in our previous work [34].

The large molecular weight fraction was separated using a Microcon® 10 kDa centrifugal filter (regenerated cellulose, 10,000 NMWL, Merck, Cork, IRL) and reconstituted in 0.5 mL ultrapure 18 MΩ water. The total Se concentration in the >10 kDa fraction was determined by ICP-MS using external calibration with carbon-matched calibration standards. The fraction was found to contain

Table 1: Instrument parameters

Laser Ablation	**NWR213**
Fluence (J·cm^{-2})	Sensitivity and homogeneity: 1, 2, 3 & 4 for Se and Fe, additionally 6 for Fe
Spot size (µm)	50 x 50
Translation rate (µm·s^{-1})	118
Repetition rate (Hz)	20
He aerosol carrier gas (L·min^{-1})	0.800
ICP-MS	**8800 (Agilent)**
Power (W)	1600
Argon make-up (L·min^{-1})	1.10 (sensitivity and homogeneity) 0.6-0.8 (methanol addition)
Torch z-position (mm)	3.6 (sensitivity and homogeneity) 5.0 (methanol addition)
Reaction cell gases	O_2: 45% H_2: 2 mL min^{-1}
Analytes (*m/z*)	^{56}Fe (56, *on-mass*), ^{57}Fe (57, *on-mass*) ^{77}Se^{16}O (93, *mass shift*),^{78}Se^{16}O (94, *mass shift*), ^{80}Se^{16}O (96, *mass shift*)
Internal standard (*m/z*)	^{32}S^{16}O (48, *mass shift*)
Dwell time (s)	0.05
Settling time (µs)	500
Concentration of methanol solution added to the laser aerosol(% v/v)	0 (dry), 1, 5, 10, 25, 50 & 100
Methanol solution flow rate (µL·min^{-1})	2.5, 5 & 10

2.0 mg·kg^{-1} Se in the reconstituted solution [68 mg·kg^{-1} in the solid extract].

As the speciation analysis of this fraction is out of the scope of this paper and has been the subject of previous papers[29, 30] it was not undertaken here.

Instrumentation

A NWR213 laser ablation platform (ESL, Huntingdon, UK), with a TV2 cell was configured such that a helium carrier gas transported ablated material to the ICP (1 m long tubing), whilst an argon make-up flow was introduced (0.25 m post cell) *via* a y-piece counter to the laser aerosol, to promote mixing. The effect of fluence on the analyte sensitivity and on the noise (within-line variation) was investigated with all other lasing parameters being held constant. The laser operation conditions are summarised in Table 1.

A 8800 ICP-MS (Agilent, Cheadle, UK) was operated under dry plasma conditions (see Table 1 for details) for standard homogeneity and species-dependent sensitivity investigations.

Tissue standard preparation and characterisation

Tissue homogenates were prepared and characterised as described by Douglas *et al* [35]. Briefly, pig brain was passed through a PTFE sieve (ca 1 mm^2 pore size) providing coarse homogenisation. Tissue was further homogenised using a Tissue Ruptor (QIAGEN, West Sussex, UK). Sub-samples of 3 g were weighed into histology moulds and spiked with varying volumes of either the inorganic salt spikes or protein species as detailed above, such that the mass of spike solution was kept <6% of the total mass, to yield Fe and Se concentration ranges of *ca* 50-2000 mg·kg^{-1} and 0.8-1.2 mg kg^{-1} (dry weight basis) respectively. This was calculated considering that the tissue homogenate weight loss by drying averaged 80 ± 1.4% (w/w; SD for n=15). Spiked tissue was homogenised using the Tissue Ruptor at 20,000 rpm for 10 minutes and centrifuged at 2000 rpm for 2 minutes to remove air pockets induced by the homogenisation, thus improving mechanical strength of tissue during sectioning. Tissue homogenates were snap-frozen by immersion in liquid N_2 for 5 minutes and stored at -80°C prior to sectioning.

Tissues were mounted in OCT (Cellpath Embedding Matrix, Fisher Scientific, Loughborough, UK) and sectioned using low profile disposable 819 blades in a CM1850 cryostat (Leica, Milton Keynes, UK), set to a temperature of -20°C, to a thickness of 30 µm. Homogeneity of the spikes at each concentration level was characterised by assessing the variation within and between ablation lines from six ablation tracks across each of the tissues. The number of points per line for comparisons of within-line and between-line variations (RSD) were 120 and 6, respectively.

Tissue Fe and Se concentration was determined from frozen blocks sub-sampled in triplicate using ICP-MS after acid digestion assisted by microwave radiation using the procedure described below. Stability of standards previously assessed over a four month period, with tissues being kept at 4 °C in the dark[31]. Stability was assessed using LA by comparing the ^{32}S-normalised sensitivity defined from the slope of the response curve.

Table 2: Microwave program for digestion of tissue homogenates.

Step	Description	Time (minutes)	Temperature (°C)
1	Ramp	15	90
2	Hold	5	90
3	Ramp	10	180
4	Hold	10	180
5	Cooling	45	-

Tissue digestion for elemental analysis by ICP-MS

Tissue Fe and Se concentration was determined from sub-sampled frozen blocks. In brief, 0.1g of frozen tissue was digested in a Milestone EthosUp system (Milestone SRL, Sorisole, Italy) using 1 mL of HNO_3 (UpA, Romil, Cambridge, UK) in PTFE micro-volume vessels, with the outer vessel containing 10 mL water and 1 mL H_2O_2 (UpA, Romil, Cambridge, UK). Digestion was achieved using the program as detailed in Table 2. Pig kidney ERM BB186 was analysed to assess accuracy of the methodology for total determination of Fe and Se.

Methanol Addition

To study the effect of carbon addition on the limit of detection obtained for Se, online addition of methanol solutions to the laser aerosol after the laser ablation cell and prior to the ICP was undertaken. This was achieved using a total consumption nebulizer (Agilent, Cheadle, UK) and a borosilicate spray chamber, similar as described by Douglas *et al* [35] for the online addition of isotopically enriched spike solution. A gas tight luer lock syringe (Agilent, Cheadle, UK) and pump (KDScientific, Massachusetts, USA) delivered solutions of 0-100 (v/v) % methanol (see Table 1 for increments and liquid flow rates) using an argon make-up gas to drive the nebuliser. Methanol solutions were prepared by mixing high purity (> 99.9 %) methanol with ultrapure 18 MΩ water. The laser aerosol carried in helium was introduced *via* the side arm of the borosilicate chamber, entering at an angle fixed towards the centre of the solution spray to promote mixing. The addition of solution to the laser induced aerosol had the added benefit of wetting the plasma, and thus providing more robust conditions[36]. For this experiment, tissue was spiked with $SeCl_4$ to yield a Se concentration of 0.48 mg·kg^{-1} in the wet solid and it was ablated (n = 5 lines) using the conditions listed in Table 1.

Results and discussion

Determination of Fe and Se in spiked tissue

The spiked tissue produced using the procedure described above was characterised for total Fe and Se concentrations using ICP-MS after microwave digestion. The determined analyte concentrations were in good agreement with the theoretical values estimated from gravimetric preparations. The average recoveries for Fe and Se from the analysis of ERM BB186 Pig Kidney were 95.5 ± 3.7 % and 92.6 ± 2.0 % (RSD, n=3), respectively. Table 3 summarises Fe and Se concentrations on a wet weight basis.

Native Fe and Se concentrations in pig brain were found to be much higher than those in lamb brain used as matrix matched standard material in previous work[27] ; approximately 3 mg kg^{-1} and 0.04 mg kg^{-1} (lamb brain), compared to 5 and 0.14 mg kg^{-1} (pig) for Fe and Se, respectively. This demonstrates again that a careful selection of background tissue for tissue matched standard preparation is crucial for the purpose of achieving limits of detection sufficiently low to undertake quantitative imaging analysis of clinical samples. This is of particular importance for Se quantification in human brain as its average concentration in healthy human brain varies between 0.05-0.1 mg·kg$^{-1,}$ depending on the brain region[14]. However, for the purpose of method development and the proof of concept presented in this work, pig brain was found suitable and, therefore, used for further experiments.

In comparison with Fe spiked standards, the relatively large RSDs (n=3) obtained for three independent digests of Se standards (up to 18%) could be attributed to the lower Se concentrations. It is important to note that the upper limit of the Se concentration used here for protein spiking is limited by the amount of water extractable Se-protein fraction from Se-yeast. Also, that the inorganic spike calibration curve is built to match the protein spike calibration curve for the purpose of a fair comparison. For both Fe and Se the standards were homogeneous over a four month period when stored at room temperature in the dark.

In order to study the effect of species-specific calibration on the quality of LA-ICP-MS data, the correlation of the calibration graph slopes (inorganic Fe *versus* ferritin-spiked) as well as the homogeneity of the calibration standards were monitored over a laser energy range of 1 to 6 J·cm^{-2}. To achieve this, transient count rates for *m/z* 56 were normalised to the transient $^{32}S^{16}O$ signal to account for variation in tissue section thickness. The backgrounds of ^{13}C and $^{31}P^{16}O$ were also monitored but suffered from a higher degree of drift than $^{32}S^{16}O$, and as such were not used for normalisation.

The investigated laser fluence ranged from values at which some ablation was observed (1J·cm^{-2}) to those at which complete ablation was achieved (3 J·cm^{-2}). The ablation threshold of glass was found to be around 4 J·cm^{-2} when using the 213 nm laser[37]. Figure 1 shows the variation of regression slopes and within-line variability for both inorganic *versus* ferritin-spiked standards with increasing laser fluence. From this figure, that the regression slopes of ferritin and $FeCl_2$ standards agree well irrespective of the laser fluence used.

Table 3: Fe and Se concentration (wet weight, background subtracted) in inorganic salt and protein- spiked tissue homogenates for 3 replicates (n=3).

Calibration Level	Fe concentration, mg kg^{-1}		Se concentration, mg kg^{-1}	
	$FeCl_2$	Ferritin	$SeCl_4$	Se-protein
1	18.8 ± 0.3	17.8 ± 0.5	0.170 ± 0.015	0.156 ± 0.017
2	28.4 ± 0.4	26.8 ± 0.1	0.184 ± 0.030	0.183 ± 0.028
3	58.0 ± 1.4	53.6 ± 1.2	0.193 ± 0.020	0.212 ± 0.030
4	204 ± 7.0	178 ± 6.0	0.218 ± 0.040	0.248 ± 0.024
5	394 ± 3.0	331 ± 3.0	n/a	n/a

Linearity of calibration graphs of both $FeCl_2$ and ferritin spiked tissue standards was excellent at fluences ≤ 3 J·cm^{-2}, being correlation coefficients between 0.9995 and 0.9999. At higher fluences, linearity decreased to 0.9971 and 0.9947 for $FeCl_2$ and ferritin respectively. A similar trend was observed for Fe homogeneity, assessed by comparing the average within-line variation (normalised to $^{32}S^{16}O$), for all analyte concentrations. It was observed that overall, within line RSDs increased as a result of increasing the laser fluence for both inorganic and protein spike species, with a larger increase observed for ferritin-spiked tissue. For fluences over 3 J cm^{-2}, at which complete ablation is achieved, mechanical liberation of tissue (observed as irregular sized pieces dislodged outside the laser ablation track), combined with the ablation of the microscope slide (resulting in non-optimum particle formation characteristics and particle size distribution) are key contributing factors to the increase of RSD. Figure 1 also shows that the lowest within-line RSD were obtained for the ferritin- spiked standards across all concentrations and laser fluences.

It is interesting to note that for ferritin spiked standards the Fe sensitivity was found to slightly decrease with the increase of laser fluence even though complete sample consumption was not achieved at the lower fluence; the Fe signal observed at 6 J·cm^{-2} being approximately 34 % lower than at 1 J·cm^{-2}. Despite this, the slopes for both species graphs seemed to agree at 6 J·cm^{-2} due to their larger associated error compared to 1 J·cm^{-2}. It would be expected that an increase in the mass flux of tissue as a result of higher laser fluence would lead to an increase in raw Fe counts detected. However, the trend observed highlights the need for signal normalisation to a suitable internal standard in order to achieve reliable quantification.

Many attempts have been made to find a suitable internal standard approach for bioimaging of tissue, but they are often dependent on the type of sample being measured and limited by the instrumentation being used. As a result, each approach has its own advantages and disadvantages [24,25,38–40]. Since this work focuses on a

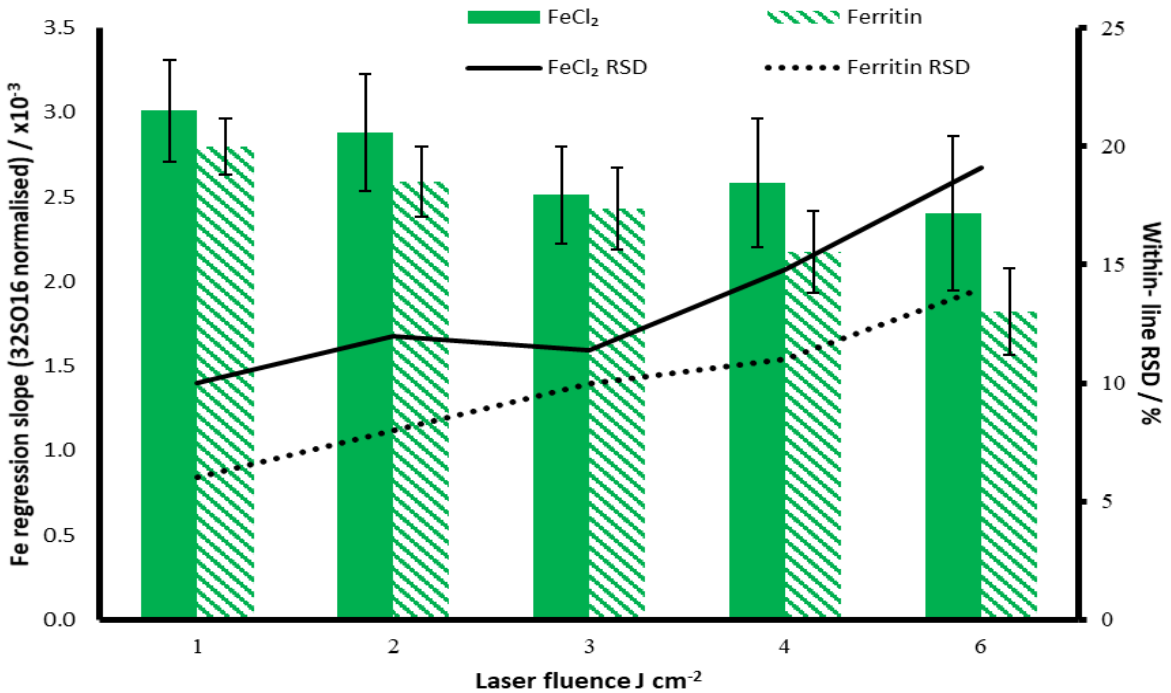

Figure 1: Species-dependent sensitivity (using $^{32}S^{16}O$ normalisation), for the inorganic spike (green bars) and the ferritin species spike (in striped bars) for each laser fluence. The black trend lines show the within-line RSD (n=120) variation with increasing laser fluence. Error bars show variation in regression slopes induced by the within-line RSD.

systematic development that requires the use of homogenized tissue-based model samples with a sufficiently high and homogeneously distributed S content (between line RSD of <15%), normalization to $^{32}S^{16}O$ was investigated for the purpose of both absolute element quantification and the correction for variation in tissue thickness between sections. The $^{32}S^{16}O$ signal stability across the duration of the measurement was found advantageous compared to other species or of similarly distributed elements such as phosphorus ($^{31}P^{16}O$) and carbon (^{13}C). This normalisation was found to be rather effective to correct for variations in tissue thickness and ablation parameters; improving the linearity of the calibration slopes when compared to the raw Fe counts. It is important to note that for future application of the developed method to real tissue samples, S will unlikely be a suitable internal standard for absolute quantitative imaging as real tissue samples are highly heterogeneous in their S content. However, for such purpose, normalisation to S would still be valuable for monitoring the performance of calibration standards prepared using homogenized tissue. The combination of reported approaches for tissue internal standardization[31,41] with the findings of this study could potentially lead to success in future work with real sample applications.

Se-proteins *versus* $SeCl_4$ spiked tissue calibration

The naturally low abundance of Se in brain[42] and the low ionisation yield of this element in an argon plasma[43], make it difficult to simultaneously quantify Se and Fe in tissue by LA-ICP-MS. In order to measure Se at biologically relevant levels, further efforts focused on achieving better limits of detection for this element.

Previous work has demonstrated that Se LOD could be improved by addition of carbon to the ICP [44,45]. Therefore, an attempt to increase the sensitivity of Se detection by adding methanol to the laser aerosol after the laser cell and prior to the ICP *via* a total consumption nebuliser, whilst avoiding any effect on Fe measurement, was undertaken. In order to achieve this, the conditions for methanol addition had to be optimised to find a balance between improving Se signal and maintaining plasma stability. Low methanol levels did not lead to sufficient signal enhancement whilst too much methanol resulted in mass loading of carbon in the ICP and causing a decrease of its robustness (increased noise and matrix effects), as well as significant signal drift due to build-up of carbon on the ICP-MS instrument interface.

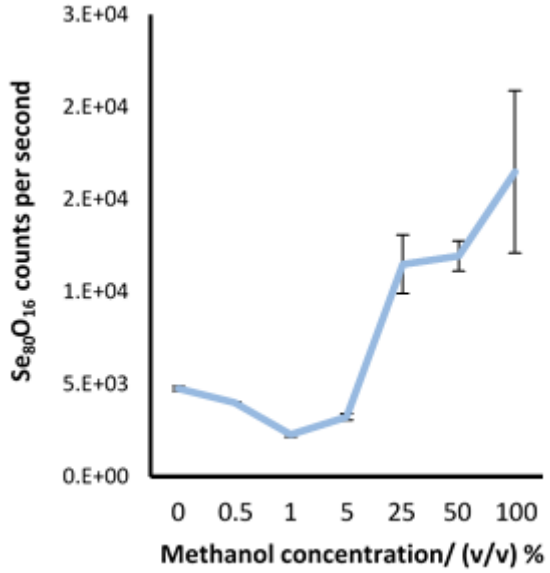

Figure 2: Sensitivity increase for $^{80}Se^{16}O$ with the addition of methanol at a flowrate of 2.5 µL min^{-1}. Error bars show the within-line variation as standard deviation (SD), n=120.

The flow rate was varied for a (v/v) 20% methanol solution concentration and both the signal to noise and the % RSD were monitored. An optimum flow rate of 2.5 µL min^{-1} was found to deliver enough carbon to the plasma for a significant sensitivity increase whilst maintaining signal stability (for 25% methanol concentration) within 5% for over a period of at least 7h.

Figure 2 shows the effect of increasing the methanol solution concentration at a flow rate of 2.5 µL min^{-1}. The Se signal increased 2.5 and 3.5 fold with the addition of 25 % and 100 % methanol, respectively. However use of 100 % methanol resulted in significant amount of carbon loading on the ICP-MS instrument interface and, therefore, signal instability, making its use an impractical choice (see enlarged error bar for 100 % methanol in Figure 2). Using 25 % methanol only a small increase in the Se background was observed, resulting in a 2-fold improvement of the Se limit of detection from 0.068 mg kg^{-1} down to 0.032 mg kg^{-1}. Under such conditions, the limit of detection obtained for Fe was 14.3 µg kg^{-1}.

The performance achieved under such conditions would make detection of both Fe and Se, at physiologically relevant concentrations, possible. To further investigate the effect of Se species-specific calibration, 25 % methanol at 2.5 µL min^{-1} was continuously added to the laser aerosol *via* a total consumption nebuliser.

Figure 3 shows the variation of both slopes (sensitivity) of inorganic versus Se-protein spike calibration as well as within-line RSDs (standard homogeneity) over a range of laser fluences (1-4 J·cm^{-2}). As shown in this figure, the choice of calibrant for Se seems to have a greater impact in comparison with Fe calibration; at 1 J·cm^{-2} the regression slope for the Se-protein calibration was approximately 36% smaller than that of inorganic Se calibration. For laser fluences over 2 J·cm^{-2} the regression slopes between the two species seem to agree within their associated measurement error, but as observed for Fe, the higher the laser fluence, the larger the within-line RSD achieved.

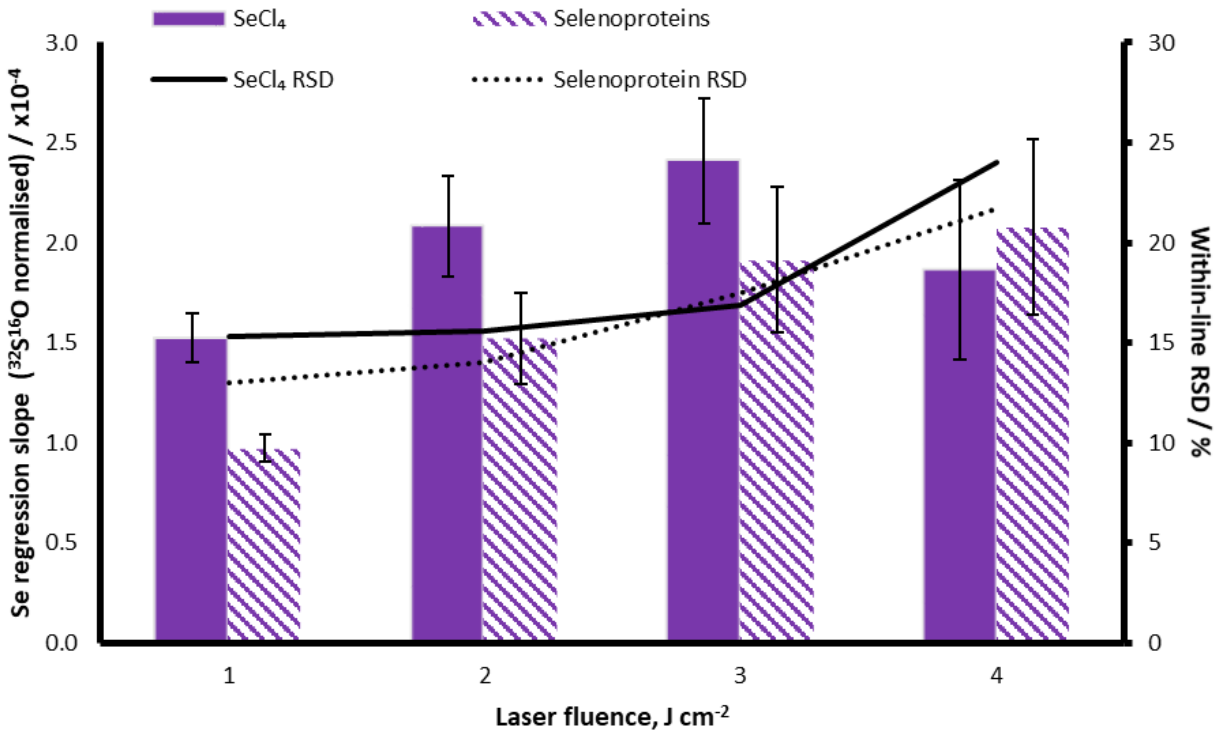

Figure 3: Species-dependent sensitivity (using $^{32}S^{16}O$ normalisation) for inorganic spike (purple) bars) and Se-protein species (striped bars) for each laser fluence. The black trend lines show the within-line RSD with increasing laser fluence. Error bars show variation in regression slopes induced by the within-line RSD (n=120).

A possible explanation for the observed difference between species is that a higher level of laser energy is required to efficiently release Se from Se-proteins and, therefore, achieve similar transport and ICP processing efficiencies in comparison with inorganic Se substrates. This hypothesis could also be supported by the fact that the Se-protein slope increases by 60 % when increasing the laser fluence from 1 to 2 J·cm^{-2}, any additional increase in laser fluence does not result in significant sensitivity increase when considering the standard deviations associated to the regression slopes. Over the same energy range the inorganic Se slope was found to only increase by 35 % (see Figure 3).

The increase in regression slope for both species with the increasing fluence above 2 J·cm^{-2} is also partially due to complete ablation of the entire tissue thickness (for a constant translation rate of 118 µm·s^{-1} using a 213 nm laser wavelength) being achieved and, thus an increase in mass flux and in the total number of Se ions. As observed for Fe, linearity of the calibration curve also improved for both Se spike species with the increasing fluence, with improved correlation coefficients from 0.9319 (1 J·cm^{-2}) to 0.9883 (3 J·cm^{-2}) and 0.9490 (1 J·cm^{-2}) to 0.9888 (3 J·cm^{-2}) for $SeCl_4$ and Se-proteins, respectively. Despite the lower concentration range of the Se calibration, the within-line RSD and, therefore, overall homogeneity of the standards are at similar levels to those for Fe.

Conclusions

Methodology for the simultaneous quantification of Fe and Se at very different concentration levels in tissue has been developed for the purpose of future application to human brain tissue and associated models. This methodology is based on tissue-matched external calibration in combination with laser ablation and ICP-MS.

For the first time the impact of elemental species-specific calibration on the accuracy of the calibration data obtained for tissue Fe and Se using laser ablation ICP-MS was investigated, and the results suggested that there is a dependency on the laser fluence working range, in particular for Se. Also, the laser fluence was found to impact the within-line RSD for both elements; overall, the higher the laser fluence, the larger the within-line RSD achieved. Therefore, careful optimisation of this laser parameter, as a compromise between achieving lowest between-line RSDs and insignificant species-specific effects, is essential in achieving high quality quantitative imaging data for both Fe and Se in a tissue matrix.

Finally, the limit of detection of Se was improved 2-fold by mixing 25% (v/v) methanol with the laser-induced aerosol in a chamber prior to introduction into the ICP, making the simultaneous detection of both elements possible at physiologically relevant concentrations.

Conflicts of interest

There are no conflicts to declare.

Author's Contribution

The following is a summary of all author contributions; Conceptualization; D.N.D, H.G.I. Formal analysis; K.B, D.N.D, G.H.S. Funding acquisition; H.G.I, J.F.C. Investigation; K.B, D.N.D, G.H.S.

Methodology: D.N.D, K.B, H.G.I. Project administration and Supervision; J.F.C, H.G.I. Resources: H.G.I. Visualisation; K.B, D.N.D. Writing-original draft: K.B, D.N.D, H.G.I. Writing-review & editing: K.B, D.N.D, G.H.S, J.F.C and H.G.I

Acknowledgements

KB thanks EPSRC and LGC for a PhD studentship co-funded through the EPSRC Centre for Doctoral Training in Molecular Analytical Science, grant number EP/L015307/1 and the UK National Measurement System Chemical and Biological Measurement and Grand Challenge Industrial Strategy Programmes from the UK Department of Business, Energy & Industrial Strategy (BEIS).

Data availability

The data that support the findings in this study are available in the Warwick Research Archive Portal (WRAP) repository, http://wrap.warwick.ac.uk

References

1 N. Braidy, A. Poljak, C. Marjo, H. Rutlidge, A. Rich, T. Jayasena, N. C. Inestrosa and P. Sachdev, *Front. Aging Neurosci.*, 2014, **6**, 138.

2 K. M. Kanninen, in *Biometals in Neurodegenerative Diseases*, 2017, pp. 415–438.

3 J. F. Collingwood and F. Adams, *Spectrochim. Acta - Part B At. Spectrosc.*, 2017, **130**, 101–118.

4 P. S. Aisen, J. Cummings, C. R. Jack, J. C. Morris, R. Sperling, L. Frölich, R. W. Jones, S. A. Dowsett, B. R. Matthews, J. Raskin, P. Scheltens and B. Dubois, *Alzheimer's Res. Ther.*, 2017, **9**, 60–69.

5 G. R. Grøntvedt, T. N. Schröder, S. B. Sando, L. White, G. Bråthen and C. F. Doeller, *Curr. Biol.*, 2018, **28**, R645–R649.

6 D. J. Piñero and J. R. Connor, *Neurosci.*, 2000, **6**, 435–453.

7 J. F. Collingwood and M. R. Davidson, *Front. Pharmacol.*, 2014, **5**, 191.

8 J. Everett, J. F. Collingwood, V. Tjendana-Tjhin, J. Brooks, F. Lermyte, G. Plascencia-Villa, I. Hands-Portman, J. Dobson, G. Perry and N. D. Telling, *Nanoscale*, 2018, **10**, 11782–11796.

9 Q. L. Xiubo Du, Chao Wang, *Curr. Top. Med. Chem.*, 2016, **16**, 835–848.

10 M. T. Zimmerman, C. A. Bayse, R. R. Ramoutar and J. L. Brumaghim, *J. Inorg. Biochem.*, 2015, **145**, 30–40.

11 N. Solovyev, E. Drobyshev, G. Bjørklund, Y. Dubrovskii, R. Lysiuk and M. P. Rayman, *Free Radic. Biol. Med.*, 2018, **127**, 124–133.

12 D. J. Piñero, J. R. Connor and G. M. Leader, *Neurosci.*, 2000, **6**, 435–454.

13 P. Ramos, A. Santos, N. R. Pinto, R. Mendes, T. Magalhães and A. Almeida, *J. Trace Elem. Med. Biol.*, 2014, **28**, 13–17.

14 P. Ramos, A. Santos, N. Rosas Pinto, R. Mendes, T. Magalhães and A. Almeida, *Biol. Trace Elem. Res.*, 2015, **163**, 89–96.

15 H. Sela, Z. Karpas, H. Cohen, Y. Zakon and Y. Zeiri, *Int. J. Mass Spectrom.*, 2011, **307**, 142–148.

16 D. N. Douglas, A. J. Managh, H. J. Reid and B. L. Sharp, *Anal. Chem.*, 2015, **87**, 11285–11294.

17 C. A. Wehe, G. M. Thyssen, C. Herdering, I. Raj, G. Ciarimboli, M. Sperling and U. Karst, *J. Am. Soc. Mass Spectrom*, 2015, **26**, 1274–1282.

18 P. K. Diwakar, J. J. Gonzalez, S. S. Harilal, R. E. Russo and A. Hassanein, *J. Anal. At. Spectrom.*, 2014, **29**, 339–346.

19 D. J. Hare, E. J. New, M. D. de Jonge and G. McColl, *Chem. Soc. Rev.*, 2015, **44**, 5941–5958.

20 M. J. Ceko, S. O'Leary, H. H. Harris, K. Hummitzsch and R. J. Rodgers, *Biol. Reprod.*, 2016, **94**, 1–14.

21 N. Miliszkiewicz, S. Walas and A. Tobiasz, *J. Anal. At. Spectrom.*, 2015, **30**, 327–338.

22 D. Pozebon, V. Dressler and G. L. Scheffler, *J. Anal. At. Spectrom.*, 2017, **32**, 890–919.

23 I. Konz, B. Fernández, M. L. Fernández, R. Pereiro and A. Sanz-Medel, *Anal. Bioanal. Chem.*, 2012, **403**, 2113–2125.

24 D. Hare, C. Austin and P. Doble, *Analyst*, 2012, **137**, 1527–1537.

25 A. Limbeck, P. Galler, M. Bonta, G. Bauer, W. Nischkauer and F. Vanhaecke, *Anal. Bioanal. Chem.*, 2015, **407**, 6593–6617.

26 D. Pozebon, G. L. Scheffler, V. L. Dressler and M. A. G. Nunes, *J. Anal. At. Spectrom.*, 2014, **29**, 2204–2228.

27 J. S. Becker, M. V Zoriy, C. Pickhardt, N. Palomero-Gallagher and K. Zilles, *Anal. Chem.*, 2005, **77**, 3208–3216.

28 C. A. Morrison, D. D. Lambert, R. J. S. Morrison, W. W. Ahlers and I. A. Nicholls, *Chem. Geol.*, 1995, **119**, 13–29.

29 D. J. Hare, J. Lear, D. Bishop, A. Beavis and P. A. Doble, *Anal. Methods*, 2013, **5**, 1915.

30 D. Pozebon, V. L. Dressler, M. F. Mesko, A. Matusch and J. S. Becker, *J. Anal. At. Spectrom.*, 2010, **25**, 1739.

31 J. O'Reilly, D. Douglas, J. Braybrook, P.-W. So, E. Vergucht, J. Garrevoet, B. Vekemans, L. Vincze and H. Goenaga-Infante, *J. Anal. At. Spectrom.*, 2014, **29**, 1378–1384.

32 R. J. Ward, F. A. Zucca, J. H. Duyn, R. R. Crichton and L. Zecca, *Lancet Neurol.*, 2014, **13**, 1045–1060.

33 J. R. Encinar, L. Ouerdane, W. Buchmann, J. Tortajada, R.

Lobinski and J. Szpunar, *Anal. Chem.*, 2003, **75**, 3765–3774.

34 H. Goenaga Infante, G. O'Connor, M. Rayman, R. Wahlen, J. Entwisle, P. Norris, R. Hearn and T. Catterick, *J. Anal. At. Spectrom.*, 2004, **19**, 1529–1538.

35 D. N. Douglas, J. O'Reilly, C. O'Connor, B. L. Sharp and H. Goenaga-Infante, *J. Anal. At. Spectrom.*, 2016, **31**, 270–279.

36 C. O 'connor, B. L. Sharp and P. Evans, *J. Anal. At. Spectrom.*, 2006, **21**, 556–565.

37 M. Guillong, I. Horn and D. Günther, *J. Anal. At. Spectrom.*, 2003, **18**, 1224–1230.

38 C. Austin, F. Fryer, J. Lear, D. Bishop, D. Hare, T. Rawling, L. Kirkup, A. McDonagh, P. Doble and D. Doble, *J. Anal. At. Spectrom.*, 2011, **26**, 1494.

39 M. Bonta, H. Lohninger, M. Marchetti-Deschmann and A. Limbeck, *Analyst*, 2014, **139**, 1521.

40 S. Hoesl, B. Neumann, S. Techritz, G. Sauter, R. Simon, H. Schlüter, M. W. Linscheid, F. Theuring, N. Jakubowski and L. Mueller, *J. Anal. At. Spectrom.*, 2016, **31**, 801–808.

41 N. Grijalba, A. Legrand, V. Holler and C. Bouvier-Capely, *Anal. Bioanal. Chem.*, 2020, **412**, 3113-3122.

42 J. Chen and M. J. Berry, *J. Neurochem.*, 2003, **86**, 1–12.

43 T. Nakazawa, D. Suzuki, H. Sakuma and N. Furuta, *J. Anal. At. Spectrom.*, 2014, **29**, 1299–1305.

44 D. Fliegel, C. Frei, G. Fontaine, Z. Hu, S. Gao and D. Günther, *Analyst*, 2011, **136**, 4925.

45 E. H. Larsen and S. Stürup, *J. Anal. At. Spectrom.*, 1994, **9**, 1099–1105.